ENVIRONMENTAL RESEARCH
LETTERS

LETTER • OPEN ACCESS

Operational differences lead to longer lifetimes of satellite detectable contrails from more fuel efficient aircraft

To cite this article: Edward Gryspeerdt *et al* 2024 *Environ. Res. Lett.* **19** 084059

ENVIRONMENTAL RESEARCH
LETTERS

CrossMark

OPEN ACCESS

RECEIVED
18 August 2023

REVISED
21 June 2024

ACCEPTED FOR PUBLICATION
25 June 2024

PUBLISHED
7 August 2024

LETTER

Operational differences lead to longer lifetimes of satellite detectable contrails from more fuel efficient aircraft

Edward Gryspeerdt[1,2,*], Marc E J Stettler[3], Roger Teoh[3], Ulrike Burkhardt[4], Toni Delovski[5], Oliver G A Driver[2] and David Painemal[6,7]

[1] Grantham Institute—Climate Change and the Environment, Imperial College London, London, United Kingdom
[2] Department of Physics, Imperial College London, London, United Kingdom
[3] Department of Civil and Environmental Engineering, Imperial College London, London, United Kingdom
[4] Deutsches Zentrum für Luft- und Raumfahrt, Institut für Physik der Atmosphäre, Oberpfaffenhofen, Germany
[5] Deutsches Zentrum für Luft- und Raumfahrt, Institut für Raumfahrtsysteme, Bremen, Germany
[6] NASA Langley Research Center, Science Directorate, Hampton, VA, United States of America
[7] Analytical Mechanics Associates Inc., Hampton, VA, United States of America
[*] Author to whom any correspondence should be addressed.

E-mail: e.gryspeerdt@imperial.ac.uk

Keywords: climate, aviation, earth-observation, aerosol, cloud

Abstract

Clouds produced by aircraft (known as contrails) contribute over half of the positive radiative forcing from aviation, but the size of this warming effect is highly uncertain. Their radiative effect is highly dependent on the microphysical properties and meteorological background state, varying strongly over the contrail lifecycle. In-situ observations have demonstrated an impact of aircraft and fuel type on contrail properties close to the aircraft, but there are few observational constraints at these longer timescales, despite these having a strong impact in high-resolution and global models. This work provides an observational quantification of these contrail controlling factors, matching air traffic data to satellite observations of contrails to isolate the role of the aircraft type in contrail properties and evolution. Investigating over 64 000 cases, a relationship between aircraft type and contrail formation is observed, with more efficient aircraft forming longer-lived satellite-detectable contrails more frequently, which could lead to a larger climate impact. This increase in contrail formation and lifetime is primarily driven by an increase in flight altitude. Business jets are also found to produce longer-lived satellite-detectable contrails despite their lower fuel flow, as they fly at higher altitudes. The increase in satellite-detected contrails behind more efficient aircraft suggests a trade-off between aircraft greenhouse gas emissions and the aviation climate impact through contrail production, due to differences in aircraft operation.

1. Introduction

Contrails, the clouds formed behind aircraft, contribute a large but highly uncertain fraction of the warming from aviation (Bock and Burkhardt 2019, Lee *et al* 2021). Forming with low optical depths (Iwabuchi *et al* 2012), they can live for hours to up to a day (Haywood *et al* 2009) and have a strong overall warming effect (Kärcher 2018). The overall climate forcing is dominated by the small fraction of aircraft that form longer-lived contrails (Burkhardt *et al* 2018, Teoh *et al* 2020). This makes aircraft-scale constraints essential to evaluate the models used to assess the climate impact of aviation (Schumann 2012), to design contrail mitigation strategies (Teoh *et al* 2020, e.g.) and to target deployment of sustainable aviation fuel (Burkhardt *et al* 2018, Teoh *et al* 2022).

Contrails form through the mixing of warm moist aircraft exhaust air with surroundings colder than the homogeneous nucleation threshold temperature. Contrail formation is predicted by the Schmidt–Appleman criterion (SAC), which for a given aircraft overall efficiency (η), fuel type and environmental relative humidity (RH) defines a threshold temperature (T_{SAC}), below which contrails can form (Schumann 1996). If the environment is supersaturated with respect to ice (RHi>100%), the ice crystals in the contrail can grow and the contrail persists.

Those that live for longer periods of time are known as long-lived contrails and are sometimes referred to as persistent contrails or contrail cirrus (when in clusters).

While there is a strong impact of background humidity on persistent contrail formation, the impact of the generating aircraft is more uncertain. Increases in the emitted non-volatile particulate matter (nvPM) number concentration are expected to produce contrails with a larger ice crystal number concentration (N_i), but with consequently smaller crystals, increasing contrail lifetime and radiative impact (Bier *et al* 2017, Kärcher 2018). Parametrised models support this, showing strong impacts of nvPM on contrail forcing (Bier and Burkhardt 2022, Teoh *et al* 2022). However, high resolution simulations indicate a smaller role for the generating aircraft, with ice crystal loss in the contrail's vortex stage significantly reducing aircraft type induced variability in persistent contrail N_i (Unterstrasser and Görsch 2014, Unterstrasser 2016).

Variations in nvPM emissions are not the only potential impact of aircraft type on contrail formation. Aircraft efficiency is related to contrail formation through variations in T_{SAC}, with more efficient aircraft having a higher T_{SAC} (typically by a few degrees; Schumann 1996), making contrail formation more likely. Contrails that form further below T_{SAC} reach higher peak supersaturations during the initial contrail formation phase, activating a larger number of ice crystals (Kärcher *et al* 2015). Model studies suggest this larger N_i increases contrail lifetime and optical depth (Burkhardt *et al* 2018). However, although chase-plane studies have shown a role of aircraft (Jeßberger *et al* 2013) and fuel (Voigt *et al* 2021) type on fresh contrails, the impact on the development and lifetime on persistent contrails has not been quantified from observations.

The similar appearance of persistent contrails to natural cirrus makes them difficult to isolate and link to the generating aircraft in observations. This typically limits insitu studies of contrails from specific aircraft to the first 10–15 min of their lifecycle, although some observations exist at longer timescales (Schumann *et al* 2017). Satellites have the capability to identify contrails over large regions (Mannstein *et al* 1999, Iwabuchi *et al* 2012, Duda *et al* 2013, 2019, Vázquez-Navarro *et al* 2015, Meijer *et al* 2022), but few studies track the evolution of contrails through their observable lifetime (Duda *et al* 2001, Haywood *et al* 2009, Vázquez-Navarro *et al* 2015, Chevallier *et al* 2023). Satellites cannot detect contrails throughout their whole lifetime (Gierens and Vázquez-Navarro 2018), but the observable lifetime can provide an approximate indication of the radiative impact of a contrail, all else being equal (Driver *et al*). However, without a link to the generating aircraft, these studies do not provide the aircraft-scale constraints essential for constraining models of persistent contrail formation and guiding future mitigation strategies.

This study addresses this gap, producing aircraft-scale constraints on the controlling factors of contrails. Contrails observed in imagery from the advanced baseline imager (ABI) onboard the Geostationary Operational Environmental Satellite (GOES-16) satellite are matched to the aircraft that formed them. Using an automatic identification algorithm, contrail-aircraft matches are identified over the western North Atlantic and tracked during the fraction of their lifetime when they are detectable from satellite. Characterising the development of independent contrail segments, the impact of aircraft type and the initial meteorological conditions are assessed, demonstrating a strong impact of both factors, providing a new database for constraining contrail simulations, and highlighting pathways to a reduction in the climate impact of aviation.

2. Methods

2.1. Data

Data from the ABI (Schmit *et al* 2017) on GOES-16 (every five minutes) is used to identify contrails over the Western North Atlantic. The eastern half of the continental US scan is used (columns 1300-2500) (figure 3), approximately the region 85° W–60° W, 15° N–50° N, due to reduced air-traffic simplifying the matching of aircraft to satellite-detected contrails. Only infra-red bands are used (band 9–6.95 μm, band 13–10.35 μm and band 15–12.3 μm), with a 2 km resolution at nadir.

Reanalysis winds, humidity and temperature were use to advect aircraft locations and characterise their formation conditions (e.g. T_{SAC}, RHi). This data was obtained from the ERA5 reanalysis at 0.25° by 0.25° resolution on pressure levels (Hersbach *et al* 2020).

Aircraft position reports were obtained from the Federal Aviation Administration's traffic flow management system (TFMS), for aircraft intersecting the New York flight information region (FIR). This provides aircraft position (longitude, latitude, altitude) updates, aircraft type information and flight number.

Representative overall efficiency (η) and non-volatile particulate matter (nvPM) for each aircraft type (and engine type where available) at cruise in the study region from the Teoh *et al* (2024) dataset, weighted by flight distance. As the TFMS output does not report aircraft tail number, engine type is matched to specific aircraft using the airline (identified from the flight number). Comparisons to the Teoh *et al* (2024) dataset shows this is more than 90% accurate for identifying engine type for the six aircraft types with multiple engine types (A320, A321, A333, B744, B788, B789). 'Business jets' are smaller jet aircraft, ICAO codes starting (C6 - Cessna Citation; CL—Bombardier Challenger; F2, F9, FA—Dassault Falcon; GL—Grumman Gulfstream/Bombardier Global Express, LJ—Learjet).

2.2. Contrail identification

Following (Mannstein *et al* 1999), algorithms for identifying contrails in satellite data (e.g. Iwabuchi *et al* 2012, Duda *et al* 2013, 2019) typically rely on three properties of contrails: contrails are linear, cold, and composed of small ice crystals. Mannstein *et al* (1999) used a set of convolutional filters on the 10 μm brightness temperature (identifying linear cold features) and the 10 μm–12 μm brightness temperature difference (using the wavelength dependence of ice crystal emissivity to identify small ice crystals).

Recent studies have demonstrated the potential for using convolutional neural networks (CNNs) for identifying contrails in satellite imagery (Meijer *et al* 2022, Ng *et al* 2023). These use a dataset of hand-identified contrails to optimise a network of convolutional filters. A variety of designs of CNN are available. In this work, we use a Res-UNet (Zhang *et al* 2018), as it has shown good performance in image-segmentation tasks and similar networks (Ronneberger *et al* 2015) have already been applied to this problem (Meijer *et al* 2022).

A training dataset of potential contrails was identified using the 10–12 μm BTD imagery. 40 images, one every 6 h between the 10th and 20th of January 2018 was checked by hand. The images were split into 128 by 128 pixel tiles and this training data was augmented using rotation and reflection transforms. 20% of the training data was held back as the test dataset (and not used for training), leaving a total of almost 53 000 tiles for training.

For each tile, the CCN only identifies contrails in the central 64 by 64 pixel region (figure 1(a)). This means that the convolutions can be used without extra padding, minimising the impact of edge effects. When a tile is at the edge of the image, valid data is reflected at the boundary (affecting approximately 35% of tiles).

The model was trained using a batch size of 128, using a weighted binary cross-entropy loss (10%–90% towards contrail locations) to cope with the imbalanced training dataset (there are many more contrail free-locations). Dropout (30%) was used to reduce over-fitting during training. Verification on the held back data produced an intersection over union of 35%. While this is lower than would be required for other tasks, an inspection of the results indicates that the CNN is identifying many contrails missed by the human-produced dataset, similar to Meijer *et al* (2022). As this CNN is not aiming to produce a complete and perfect dataset of contrails, it is sufficient for this study, with the remaining false positives removed through stringent post-processing.

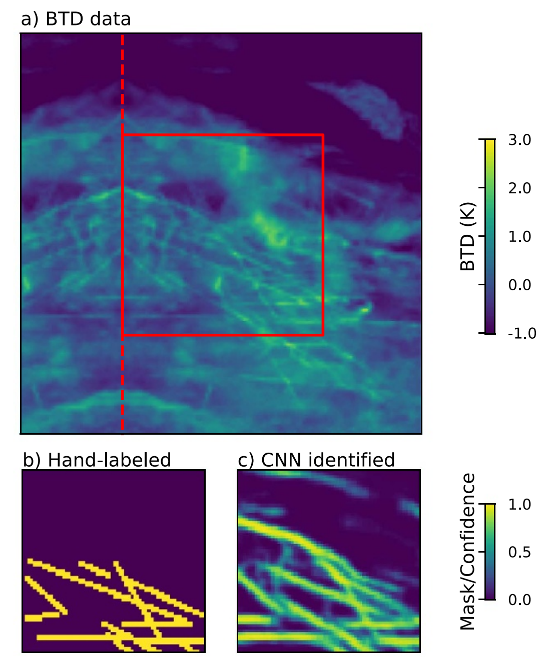

Figure 1. An example identification case. (a) Shows the 10.8 μm–13 μm BTD. All the data in the visible region is used for the model, which identifies contrails in the central region (outlined by the red box). In cases where the identification region is at the edge of the GOES image (the dashed red line in this case), the outer region is generated by reflecting the data within the region. (b) The hand identified contrails within the identification region. (c) The contrails identified by the CNN (confidence in the range 0–1).

2.3. Post-processing contrails

As with previous studies, the CNN has a considerable false positive rate. While this is partly due to the CNN identifying contrails missed by the hand-identification stage, some of these false identification are linear cloud features, natural cirrus and surface features (notably rivers). Further post-processing is applied to increase confidence in the contrail identification.

A binary contrail mask is created for each ABI image (every 5 min), with a 50% confidence threshold in the CCN output identifying contrail pixels. The mask is then split into four-connected 'contrail objects' (COs). A CO that exists for only one image (defined as not overlapping with a CO in either the preceding or following image) is removed as a likely false positive. The individual images COs are linked between images to create time-dependent objects by advecting them with the 175 hPa winds

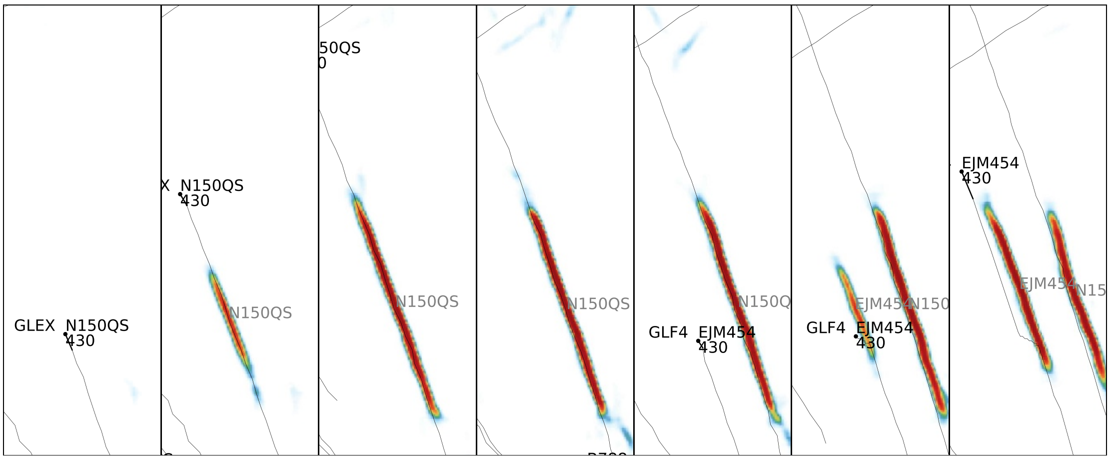

Figure 2. An example labelling of a contrail object (CO) over the Bahamas. Colours indicate the CNN confidence, from low (white/blue) to high (red). Following the passage of flight N150QS (black dot), a potential contrail formation location (PCFL) is identified by advecting historical aircraft locations using horizontal reanalysis winds. Shortly behind N150QS, a CO is identified in satellite imagery and unambiguously matched to N150QS. The development of the CO is followed until it dissipates one hour after formation. Each panel is separated by 10 min.

(approximately the flight level for commercial jets), resetting the CO location in each image to reduce the cumulative impact of errors in reanalysis winds (similar to Vázquez-Navarro *et al* 2015). This also helps to remove the surface feature false positives (figure 3(b)).

COs are then matched to aircraft from the TFMS dataset, correcting for parallax. Potential contrail formation locations (PCFLs) are identified for each aircraft by advecting aircraft positions with ERA5 flight-level winds (allowing COs to be matched as long as the form within 2 h of the aircraft passage). For a CO to be assigned to a particular aircraft, it must:

- Appear behind the aircraft, with no component appearing before the passage of the aircraft
- Have an aspect ratio of 3 or more and be aligned with the PCFL within 30 degrees
- Have a centre less than 6 km from the PCFL

If multiple aircraft satisfy these criteria, the aircraft with the closest position match between the CO and PCFL is assigned to that CO. As the TFMS dataset is not complete, there is a possibility of excluded flights forming contrails which are observed and matched to other aircraft. The matching criteria limit this possibility, as the excluded aircraft would have to fly at the same direction and altitude as another aircraft within the 10–15 min it takes a contrail to be detected.

This method produces matches (figure 2) between aircraft and COs. The CO maintains the aircraft identity until it disappears (no longer overlaps with an advected CO in the following image), which then defines the end of the lifecycle of the CO. For cases where a CO splits, the child COs maintain the same aircraft identity. CO merges take the identity of the larger original CO, but are usually removed by the linearity requirements unless they are both from the same aircraft. For the whole of 2018, this produces over 120 000 COs in the study region.

Even with this matching to flight tracks, false positives remain (figure 3(b)); further filtering is required to increase confidence in the aircraft-CO matches. These COs must maintain a linear shape throughout their observed lifetime and first become visible to the CNN no more than 30 min behind the aircraft. These more stringent requirements reduce the number of contrail objects to 9604 COs, where the aircraft is linked to the observed contrail lifecycle.

Each CO is split into segments that are each one minute of flight time long (around 10–14 km), which are then used for analysis. 64 046 distinct contrail segments are analysed in this work

3. Results

3.1. Contrail identification

Contrails are identified in ABI imagery using a CNN (Ronneberger *et al* 2015), producing an observed distribution of contrails (figure 3(a)) that is qualitatively similar to previous studies (e.g. Meijer *et al* 2022). Contrails are often observed over continental North America and the North Atlantic (figure 3(a)), due to the higher frequency of air traffic (Digby 2021) and the ends of the North Atlantic Tracks. High-altitude oceanic flight corridors are visible, both between the United States and the Caribbean as well as around the Bahamas and Bermuda. Large patches of contrails are observed to the west of Florida, and north-east of Cuba (figure 3(a)), both easily visible in satellite imagery of individual days.

Coastlines, rivers and other thin, approximately linear surface features are also identified as contrails by the CNN due to their variations in emissivity (the physical basis of the brightness temperature difference method). Satellite artefacts are also visible as

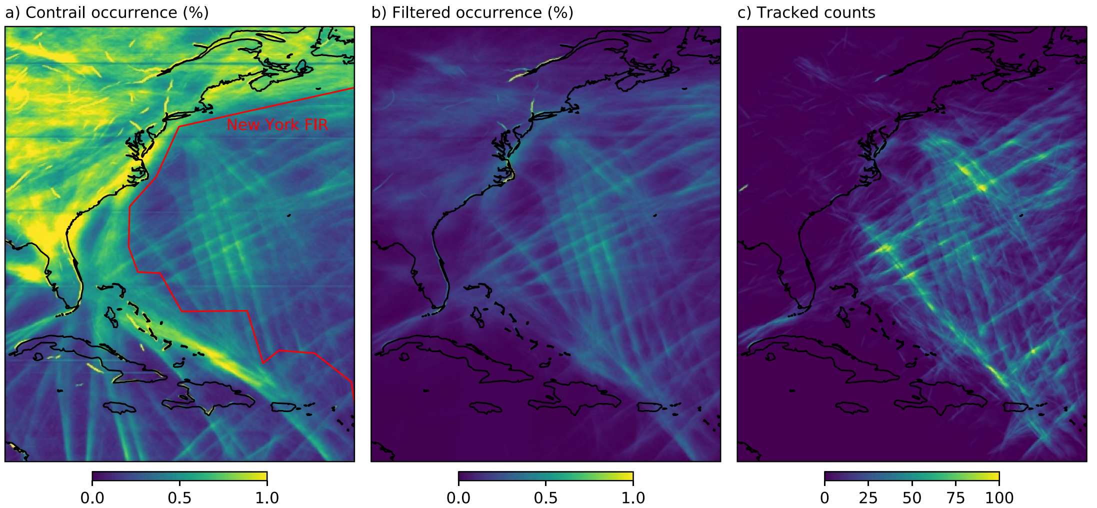

Figure 3. (a) The probability of a contrail object (CO) during 2018. (b) as (a) but only for COs linked to a specific flight (note the comparative lack of data outside the New York FIR). (c) The number of high-confidence flight-linked COs selected for tracking and further analysis.

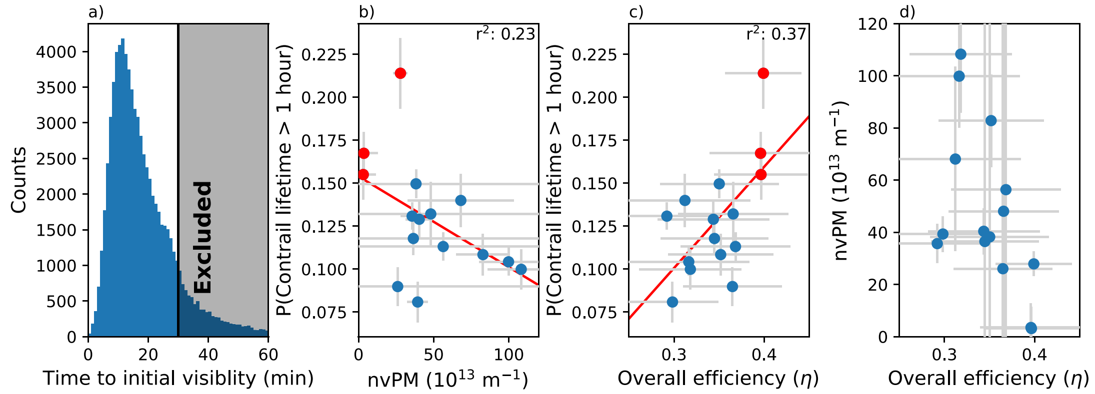

Figure 4. (a) Time to CO observation following the passage of the generating aircraft. COs with a time to observation longer than 30 min are excluded from the analysis as the aircraft match is less certain. (b) Relationship between CO observable lifetime (P(lifetime>1hour)) and nvPM emissions (one dot per aircraft/engine combination). Red dots are Type B variations. (c) As (b), but the relationship between CO lifetime and overall efficiency. (d) The relationship between nvPM and overall efficiency, averaged by aircraft type.

horizontal lines in figure 3(a). While these can be removed using maps of surface features (e.g. Meijer *et al* 2022), tracking the motion of contrails over time (see Material and methods) to form contrail objects (CO) and requiring these COs to appear only after the passage of an aircraft and to be advected with the high level winds removes most of the surface features (figure 3(b)).

The surface features can still merge with a CO over time, such that some features (such as the Hudson river) remain in regions with high frequencies of aircraft traffic. The remaining surface features are almost completely removed when the linearity conditions are imposed throughout the CO observable lifetime (figure 3(c)). This restricts the CO population to only COs that have a high confidence of being contrails, both through their behaviour and strength of the their match to an individual flight. The remaining COs are primarily over ocean, due to the improved quality of the CCN identification for cases with a simple background and the lower density of flights preventing overlapping contrails.

3.2. Observation timescales

While the nature of the CNN detection uses some non-local information, contrails do not transmit information along their length. Each CO is therefore considered as a chain of independent contrail 'segments' throughout the remainder of this work. While the matching criteria require a CO to appear less than two hours behind an aircraft, the majority (77%) of contrails segments in this region are visible in ABI imagery within 20 min (figure 4(a)), with

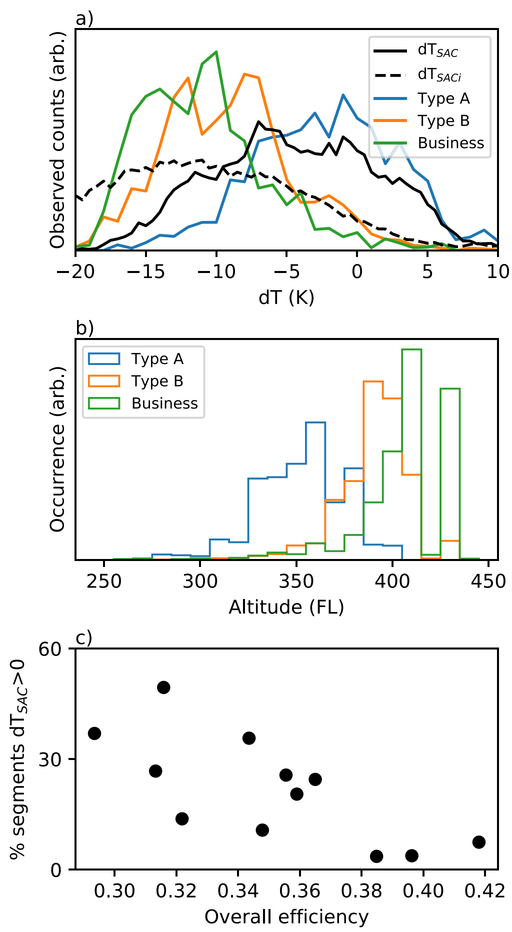

Figure 5. (a) Contrail segment occurrence by dT_{SAC} and aircraft type. Black lines are for all aircraft, the dashed black line is dT_{SAC} assuming contrails form at ice (rather than liquid) supersaturation. Each line if formed from total number of counts in dT_{SAC} bins of 1 K, normalised by the total number of counts. (b) Normalised histograms showing the altitude of the generating aircraft for each contrail segment by aircraft type. (c) Probability of a contrail being observed at temperatures warmer than T_{SAC} as a function of overall efficiency. Each dot represents a single aircraft-engine type combination.

only 4% becoming visible within the first 5 min, giving a mean time to observation of 17 min, disappearing an average of 51 min after the passage of the aircraft. Discarding segments with a time to observation of longer than 30 min (due to the uncertainty of the aircraft match) reduces these to 14 min (to first observation) and 49 min (to disappearance).

The mean lifetime (period observable in satellite data) is highly skewed by a small number of long-lifetime contrails, so the probability of an observed contrail lasting more than one hour is presented to minimise the impact of these outliers (figure 4(b)). Binning contrails by aircraft type (and engine type where available) and selecting only those types with more than 1000 segments, the parametrised particulate emissions of the aircraft (represented by the nvPM—non-volatile particulate matter emissions, from Teoh *et al* 2024) are found to be weakly negatively (but significantly) correlated with persistent contrail lifetimes. This is in contrast to recent modelling studies, where aircraft with higher nvPM emissions produced longer lived contrails with larger radiative or energy forcings (Burkhardt *et al* 2018, Bier and Burkhardt 2022, Teoh *et al* 2022).

In contrast, aircraft type overall efficiency (averaged by type) is positively correlated to contrail lifetime, with more efficient aircraft producing longer lived contrails (figure 4(c)). Although newer, more efficient aircraft typically have lower nvPM emissions (figure 4(d)), the expected reduction in contrail lifetime is not observed. Instead, the increase in contrail lifetime for these more efficient aircraft is dominated by differences in meteorology at their operating altitudes.

3.3. Meteorological factors

While the SAC defines the conditions for contrail formation, a significant number of contrails are observed to form above T_{SAC}, with a positive dT_{SAC} (ambient temperature—T_{SAC} difference; figure 5(a). This could be due to the relatively coarse (approximately 25 km) resolution of the meteorological reanalysis used in the T_{SAC} calculation neglecting the variability inherent in the temperature and humidity fields (Sundqvist *et al* 1989, Burkhardt *et al* 2008, Quaas 2012). Along with these random errors producing positive dT_{SAC}, low resolution models often have temperature biases in the upper troposphere and the supersaturated layers necessary for forming persistent contrails are often thin (Spichtinger *et al* 2003, Rädel and Shine 2008, Gierens *et al* 2020), making them difficult to represent (Agarwal *et al* 2022). These factors may also produce positive dT_{SAC}. Note that if T_{SAC} is calculated relative to ice supersaturation (figure 5(a)—dashed line), all contrails are below this threshold temperature, indicating that all the observed contrails can at least transiently achieve the ice supersaturation required for persistent contrails. Small-scale fluctuations in humidity or aircraft characteristics could locally produce the water saturation necessary to form contrails, which may persist even in slightly sub-saturated air (Li *et al* 2023).

The fraction of contrails with $dT_{SAC} > 0$ (indicating how close contrails are to the formation threshold), depends on aircraft type. Two indicative types shown in (figure 5(a)). The two types are wide-body aircraft from the same manufacturer with similar sizes, but very different fleet average ages (Type A $\approx$ 25 years, Type B $\approx$ 5 years) and mean η (Type A - 0.34, Type B - 0.40). The contrails observed from more efficient Type B are typically at lower (more negative) values of dT_{SAC}. This is expected (more efficient engines produce cooler exhaust and hence a steeper mixing line and higher T_{SAC}) and

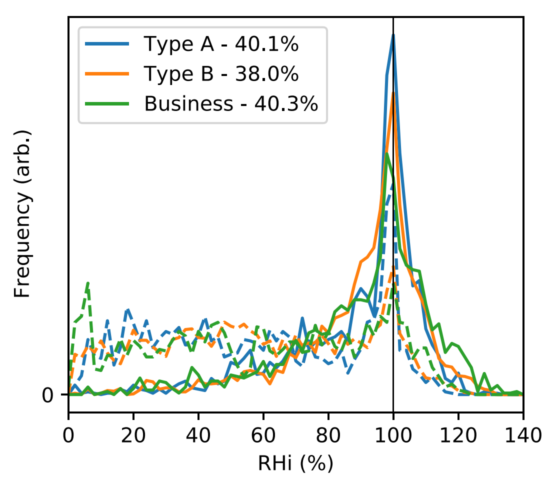

Figure 6. Contrail occurrence as a function of RHi for different aircraft types. Dashed lines are using a mismatched year for the RHi data but the same satellite observed contrails, showing the average RHi distribution at aircraft flight altitudes. The probability of RHi>100% for each type is shown in the legend.

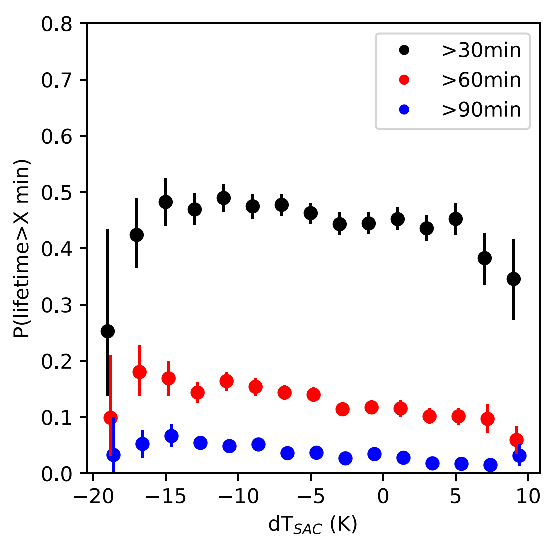

Figure 7. Probabilities of contrail segment lifetimes exceeding 30 (black), 60 (red) and 90 min(blue) as a function of the initial dT_{SAC}. Statistical uncertainties at the 5%–95% level are shown as errorbars.

there is also some evidence that the T_{SAC} is inaccurate for high bypass engines, making the wrong assumptions about η (Nieuwerth 2023). However, the changes in T_{SAC} from a 20% increase in η is around 2–4 K (Schumann 1996). Variations in T $_{SAC}$ are also produced through changes in pressure (1–2 K) and potential biases in humidity (up to 5 K). These dT_{SAC} variations too small to explain the >10 K differences in dT_{SAC} between aircraft types found in this study (figure 5(a)). This relationship remains across many different aircraft types (figure 5(c)), with as much as 50% of all contrails being apparently above T_{SAC} for some aircraft types.

This difference in dT_{SAC} between aircraft types is due to varying operating altitudes. Aircraft with a lower (more negative) dT_{SAC} are typically flying at higher altitudes (figure 5(b)). In the study region, Type B cruises at a higher average altitude (around FL400 = 40 000 ft) than Type A (FL370). Business jets usually cruise at even higher (>FL410, figure 5(b)) and colder altitudes. As temperatures at these altitudes are typically cooler, the contrails formed are usually even further below T_{SAC}.

3.4. Humidity variations

Supersaturation over ice (RHi>100%) is required for the formation of persistent contrails. A higher mean reanalysis RHi may indicate larger super-saturated regions at a sub-gridscale (Sundqvist *et al* 1989) and so might be expected to produce longer-lived contrails. For a given temperature, a higher RHi also means a larger T_{SAC} and hence more negative dT_{SAC}. With RHi variability generating correlated changes in contrail lifetime and dT_{SAC}, it is not clear that the initial dT_{SAC} is itself generating a longer lifetime contrail through increased N_i.

However, although the aircraft fly at a range of altitudes, there is little difference in the RHi at contrail formation for the different types (figure 6). For all types, there is a peak in RHi for observed contrails at saturation (100%). This is expected, as the reanalysis data lowers any supersaturated RHi to 100% in the presence of a cloud (ECMWF 2016). A considerable fraction of contrails are also observed below saturation, similar to Li *et al* (2023). However, the lack of a strong link between RHi and aircraft type (with little variation in the probability of RHi>100%) suggests RHi differences are not responsible for the variations in contrail lifetime and occurrence, although a altitude-dependent bias in RHi may mean that the RHi impact is unobserved in this work.

These contrails are all long-lived contrails (persisting longer then 10 min after the passage of the aircraft), which require a super-saturated environment to avoid dissipation. The occurrence of persistent contrails in highly sub-saturated environments highlights the limitations of reanalysis RHi for contrail prediction (Rädel and Shine 2008, Gierens *et al* 2020, Agarwal *et al* 2022). However, the RHi distribution is very different from the average RHi in this location (estimated using RHi from a mismatched year, figure 6—dashed lines) indicating that the reanalysis product still has some skill at predicting the RHi.

3.5. Meteorology and contrail lifetime

Although there is not a clear link between contrail lifetime and RHi, contrail lifetime is linked to the initial contrail formation conditions through dT_{SAC} (figure 7). Colder contrails (those forming further below dT_{SAC}) have a longer lifetime, approximately doubling the chance of a contrail segment living longer than an hour if the contrail forms at 20 K below T_{SAC}, compared to one forming close to T_{SAC} (figure 7, blue dots). This is consistent with contrails forming closer to T_{SAC} having fewer, larger crystals (Kärcher *et al* 2015) and the faster growth of ice crystals in warmer conditions producing higher sedimentation rates, reducing contrail lifetimes (Bier *et al* 2017). Where a lower dT_{SAC} indicates contrails forming close to the tropopause, the increased size of supersaturated regions may also play a role by allowing a contrail to last longer at high humidity (Burkhardt *et al* 2008).

This dT_{SAC} link to contrail lifetime dominates the link between aircraft type and contrail lifetime (figures 4(b) and (c)) to such an extent that no clear link is found to lifetime for either overall efficiency or nvPM emissions when binning by dT_{SAC} (not shown). While this does not preclude a link and impact on contrail properties and forcing, further studies are required to assess this effect in observations.

3.6. Fleet-wide contrails

The contrails studied in this work are a small subset of all contrails formed in the atmosphere. Stringent filtering to match aircraft to contrails limits this further to contrails that form large linear, satellite-identifiable features. The linearity criterion also biases the previous results to oceanic regions with less air traffic to reduce overlap between contrails. These sampling biases may be partly responsible for the difference in contrail development between different aircraft.

Using the advected flightpaths to identify potential aircraft-modified clouds (e.g. Tesche *et al* 2016, Duda *et al* 2019, Marjani *et al* 2022, Chevallier *et al* 2023) avoids the requirement for tracking COs and potential selection biases associated with the filtering and tracking processes. Although the CNN produces a considerable number of false positives (figure 3(a)), these are significantly reduced over the ocean. Subtracting the probability of intersection with flights from a different year accounts for random intersections and further reduces the impact of these false positives. The increased reliance on advected winds (rather than tracking the COs themselves) magnifies potential biases from errors in the reanalysis winds, which may in turn create biases in the apparent contrail lifetime.

Even with these caveats, the probability of an advected flightpath intersecting with a CNN-identified contrail still varies significantly by aircraft type (figure 8). Type B aircraft intersect with CNN-identified contrails far more often than Type A or business jets, supporting previous results that the Type B produces satellite-detectable contrails more frequently. As similar sized aircraft, both Type A and B quickly produce visible contrails (peaking at about 10–15 min behind the aircraft). Business jets take longer to produce visible contrails (peaking at about 20 min behind the aircraft), potentially due to their smaller fuel flow, engines, plume widths and contrail optical depths.

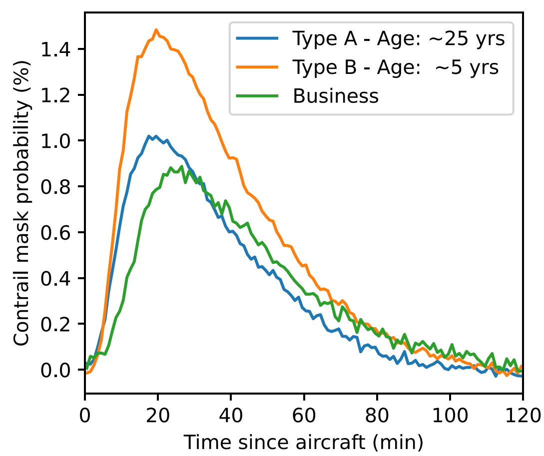

Figure 8. Probability of advected aircraft locations intersecting with contrails as identified by the CNN for different aircraft types.

The accuracy of the detectable contrail lifetime derived from figure 8 depends on the accuracy of the aircraft-altitude winds. However, business jets have a similar peak magnitude in contrail detection probability to Type A, but with a significantly longer lifetime, comparable to Type B. Even including potential false positives from the CNN identification, this supports the other results in this work, demonstrating that they are not purely due to a selection bias from the CO filtering criteria, but an actual consequence of the aircraft and their flight patterns.

4. Discussion and conclusions

More efficient aircraft generate contrails with longer satellite-detectable lifetimes (figure 4(c)) due to differences in their operation and despite a reduction in nvPM emissions that would be expected to reduce contrail lifetime (Burkhardt *et al* 2018, Kärcher 2018). Flying at higher altitudes (figure 5(b)), these more efficient aircraft form contrails further below the Schmidt–Appleman threshold temperature (T_{SAC}; figure 5(a)). While there is not a strong link between aircraft type and the environmental RH or supersaturation frequency (figure 6), contrail lifetimes increase as dT_{SAC} decreases, demonstrating an impact of the contrail initial state on the properties and lifetime of the contrail.

For the subset of contrails analysed in this work, more efficient aircraft produce longer-lived contrails, but as a consequence of the environment they fly in. While this disguises the hypothesised impact of nvPM on contrail lifetime (Burkhardt *et al*

2018, Kärcher 2018), figure 4 hints at an nvPM impact on contrail lifetime for a single type. The three red points in figure 4 are variants of Type B, with similar overall efficiencies (η; figure 4(c)), sizes (Unterstrasser and Görsch 2014) and flight profiles. The reduction in nvPM emissions for the Type B variants hints at a reduction in contrail lifetime (figure 4(b)). This highlights a potential pathway for mitigating the climate impacts of aviation, providing initial observational evidence to support results from model studies (Burkhardt *et al* 2018, Teoh *et al* 2022).

It should be noted that the aircraft in the region used in this work typically fly in the troposphere ($\lesssim$14 km in this region), rather than the drier stratosphere (as common further north). This likely increases the frequency of the persistent contrails observed in this work due to the higher tropospheric RH, particularly just below the tropopause. Further studies are required to assess these results for other regions particularly for locations such as the North Atlantic Tracks, where stratospheric flights are more common.

This study is also limited to contrails detectable in satellite data. These contrails have to live long enough, grow wide enough and achieve a high enough optical depth (Kärcher *et al* 2009) for identification (approx 10 min; figure 4(a)) and have a linear shape. While most contrails keep a linear shape given their long length and comparatively small width, this biases the study towards larger supersaturated regions. In addition, if higher altitude contrails are significantly easier to detect, this may also bias the results of this work. However, as the BTD method depends on a contrast in emissivity variations with wavelength, rather than temperature, the impact of this bias is likely small, but will be investigated in future work.

While the BTD method used to identify contrails has a long history (e.g. Mannstein *et al* 1999), it may not identify all of the most climatically relevant contrails, making the conversion to a net climate impact for each aircraft type not straightforward. As satellite detectable contrails have a larger width and optical depth, changes in the detectable lifetime might be expected to indicate a changed climate impact. However, we cannot directly observe the radiative properties of the contrails over their whole lifecycle. It is possible that the observed change in the satellite-detectable contrail lifetime is offset by opposite changes in undetected contrails and so does not produce a radiative impact.

Further work is required to assess this possibility, but it would require significant variation in undetected contrails in the opposite direction to the behaviour of the satellite-detected contrails. However, as Type B aircraft are producing much more common, longer lived satellite-detected contrails (figure 8), this is likely to lead to a larger climate impact. As erroneous matches between aircraft and observed contrails would be expected to reduce the significance of this variation with aircraft type, such that the type-dependence of detected contrail lifetime could be even larger than found in this work.

This work provides some initial evidence consistent with a reduction in nvPM emissions leading to a reduction in contrail lifetime for a single aircraft type (figure 4(b), red dots), but that this is obscured by differences in operation of different aircraft types. While higher altitude flights can be more fuel efficient, these flights typically produce contrails with longer detectable lifetimes, consistent with a larger climate impact (figures 5 and 7) and illustrating a tradeoff in the climate impact of aviation. This is particularly severe for business jets, which fly at higher altitudes and so form contrails at even lower values of dT_{SAC} than the most efficient commercial aircraft (figure 5(a)). Formed at cold temperatures, with more ice crystals and potential longer lifetimes (figure 8), this gives them a larger climate impact per passenger than their greenhouse gas emissions suggest. These potential tradeoffs between the climate effect of contrails and aircraft fuel efficiency should be carefully considered in order to meet future aviation climate targets.

Data availability statement

The GOES data were obtained through the Google Cloud Marketplace. The ERA5 data were obtained from the Climate Data Store (CDS) of the Copernicus Climate Change Service. The aircraft location data was obtained from the Federal Aviation Administration.

Acknowledgment

The authors thank Charles Harvey for his assistance with JavaScript. EG was supported by a Royal Society University Research Fellowship (Grant No. URF/R1/191602). OGAD was supported by the EPSRC Centre for Doctoral Training in Aerosol Science (EP/S023593/1). DP acknowledges support from the NASA Atmospheric Composition Campaign Data Analysis and Modeling Program.

ORCID iDs

Edward Gryspeerdt https://orcid.org/0000-0002-3815-4756
Marc E J Stettler https://orcid.org/0000-0002-2066-9380
Ulrike Burkhardt https://orcid.org/0000-0002-0742-7176
Toni Delovski https://orcid.org/0000-0003-4228-3830
Oliver G A Driver https://orcid.org/0000-0003-4444-7376
David Painemal https://orcid.org/0000-0002-1281-4672

References

Agarwal A, Meijer V R, Eastham S D, Speth R L and Barrett S R H 2022 Reanalysis-driven simulations may overestimate persistent contrail formation by 100%–250% *Environ. Res. Lett.* **17** 014045

Bier A and Burkhardt U 2022 Impact of parametrizing microphysical processes in the jet and vortex phase on contrail cirrus properties and radiative forcing *J. Geophys. Res.* **127** e2022JD036677

Bier A, Burkhardt U and Bock L 2017 Synoptic control of contrail cirrus life cycles and their modification due to reduced soot number emissions *J. Geophys. Res.* **122** 11584–603

Bock L and Burkhardt U 2019 Contrail cirrus radiative forcing for future air traffic *Atmos. Chem. Phys.* **19** 8163–74

Burkhardt U, Bock L and Bier A 2018 Mitigating the contrail cirrus climate impact by reducing aircraft soot number emissions *npj Clim. Atmos. Sci.* **1** 37

Burkhardt U, Kärcher B, Ponater M, Gierens K and Gettelman A 2008 Contrail cirrus supporting areas in model and observations *Geophys. Res. Lett.* **35** L16808

Chevallier R, Shapiro M, Engberg Z, Soler M and Delahaye D 2023 Linear contrails detection, tracking and matching with aircraft using geostationary satellite and air traffic data *Aerospace* **10** 578

Digby R 2021 FlightRadar24 Aviation Density for 2019/20 (Borealis) (https://doi.org/10.5683/SP2/ZGGYVO)

Driver O G A, Stettler M E J and Gryspeerdt E Factors limiting contrail detection in satellite imagery submitted

Duda D P, Bedka S T, Minnis P, Spangenberg D, Khlopenkov K, Chee T and Smith Jr. W L 2019 Northern Hemisphere contrail properties derived from Terra and Aqua MODIS data for 2006 and 2012 *Atmos. Chem. Phys.* **19** 5313–30

Duda D P, Minnis P, Khlopenkov K, Chee T L and Boeke R 2013 Estimation of 2006 Northern Hemisphere contrail coverage using MODIS data *Geophys. Res. Lett.* **40** 612–7

Duda D P, Minnis P and Nguyen L 2001 Estimates of cloud radiative forcing in contrail clusters using GOES imagery *J. Geophys. Res.* **106** 4927–37

ECMWF: IFS Documentation CY41R2 - Part IV: Physical Processes 2016 ECMWF

Gierens K, Matthes S and Rohs S 2020 How well can persistent contrails be predicted? *Aerospace* **7** 169

Gierens K and Vázquez-Navarro M 2018 Statistical analysis of contrail lifetimes from a satellite perspective *Meteorol. Z.* **27** 183–93

Haywood J M, Allan R P, Bornemann J, Forster P M, Francis P N, Milton S, RäDel G, Rap A, Shine K P and Thorpe R 2009 A case study of the radiative forcing of persistent contrails evolving into contrail-induced cirrus *J. Geophys. Res.* **114** D24 201

Hersbach H *et al* 2020 The ERA5 global reanalysis *Q. J. R. Meteor. Soc.* **146** 1999–2049

Iwabuchi H, Yang P, Liou K N and Minnis P 2012 Physical and optical properties of persistent contrails: climatology and interpretation *J. Geophys. Res.* **117** D06 215

Jeßberger P, Voigt C, Schumann U, Sölch I, Schlager H, Kaufmann S, Petzold A, Schäuble D and Gayet J-F 2013 Aircraft type influence on contrail properties *Atmos. Chem. Phys.* **13** 11965–84

Kärcher B 2018 Formation and radiative forcing of contrail cirrus *Nat. Commun.* **9** 1824

Kärcher B, Burkhardt U, Bier A, Bock L and Ford I J 2015 The microphysical pathway to contrail formation *J. Geophys. Res.* **120** 7893–927

Kärcher B, Burkhardt U, Unterstrasser S and Minnis P 2009 Factors controlling contrail cirrus optical depth *Atmos. Chem. Phys.* **9** 6229–54

Lee D *et al* 2021 The contribution of global aviation to anthropogenic climate forcing for 2000 to 2018 *Atmos. Environ.* **244** 117 834

Li Y *et al* 2023 Upper-tropospheric slightly ice-subsaturated regions: frequency of occurrence and statistical evidence for the appearance of contrail cirrus *Atmos. Chem. Phys.* **23** 2251–71

Mannstein H, Meyer R and Wendling P 1999 Operational detection of contrails from NOAA-AVHRR-data *Int. J. Remote Sens.* **20** 1641–60

Marjani S, Tesche M, Bräuer P, Sourdeval O and Quaas J 2022 Satellite observations of the impact of individual aircraft on ice crystal number in thin cirrus clouds *Geophys. Res. Lett.* **49** e2021GL096173

Meijer V R, Kulik L, Eastham S D, Allroggen F, Speth R L, Karaman S and Barrett S R H 2022 Contrail coverage over the United States before and during the COVID-19 pandemic *Environ. Res. Lett.* **17** 034 039

Ng J Y-H, McCloskey K, Cui J, Meijer V R, Brand E, Sarna A, Goyal N, Arsdale C V and Geraedts S 2023 Opencontrails: benchmarking contrail detection on GOES-16 ABI (arXiv:2304.02122)

Nieuwerth G 2023 Exploring options for improving prediction methods on the formation of contrails from modern turbofan engines *Master's Thesis* TU Delft

Quaas J 2012 Evaluating the "critical relative humidity" as a measure of subgrid-scale variability of humidity in general circulation model cloud cover parameterizations using satellite data *J. Geophys. Res.* **117** 09 208

Rädel G and Shine K P 2008 Radiative forcing by persistent contrails and its dependence on cruise altitudes *J. Geophys. Res.* **113** D07105

Ronneberger O, Fischer P and Brox T 2015 U-Net: convolutional networks for biomedical image segmentation *CoRR* (arXiv:1505.04597)

Schmit T J, Griffith P, Gunshor M M, Daniels J M, Goodman S J and Lebair W J 2017 A closer look at the ABI on the GOES-R Series *Bull. Am. Meteorol. Soc.* **98** 681–98

Schumann U 1996 On conditions for contrail formation from aircraft exhausts *Meteorol. Z.* **5** 4–23

Schumann U 2012 A contrail cirrus prediction model *Geosci. Model Dev.* **5** 543–80

Schumann U *et al* 2017 Properties of individual contrails: a compilation of observations and some comparisons *Atmos. Chem. Phys.* **17** 403–38

Spichtinger P, Gierens K and Read W 2003 The global distribution of ice-supersaturated regions as seen by the Microwave Limb Sounder *Q. J. R. Meteor. Soc.* **129** 3391–410

Sundqvist H, Berge E and Kristjánsson J E 1989 Condensation and cloud parameterization studies with a mesoscale numerical weather prediction model *Mon. Weather Rev.* **117** 1641–57

Teoh R, Engberg Z, Shapiro M, Dray L and Stettler M 2024 The high-resolution Global Aviation emissions Inventory based on ADS-B (GAIA) for 2019–2021 *Atmos. Chem. Phys.* **24** 725–44

Teoh R, Schumann U, Gryspeerdt E, Shapiro M, Molloy J, Koudis G, Voigt C and Stettler M E J 2022 Aviation contrail climate effects in the North Atlantic from 2016 to 2021 *Atmos. Chem. Phys.* **22** 10 919–10 935

Teoh R, Schumann U, Majumdar A and Stettler M E J 2020 Mitigating the climate forcing of aircraft contrails by small-scale diversions and technology adoption *Environ. Sci. Technol.* **54** 2941–50

Tesche M, Achtert P, Glantz P and Noone K J 2016 Aviation effects on already-existing cirrus clouds *Nat. Commun.* **7** 12 016

Unterstrasser S 2016 Properties of young contrails; a parametrisation based on large-eddy simulations *Atmos. Chem. Phys.* **16** 2059–82

Unterstrasser S and Görsch N 2014 Aircraft-type dependency of contrail evolution *J. Geophys. Res.* **119** 14,015–14,027
Vázquez-Navarro M, Mannstein H and Kox S 2015 Contrail life cycle and properties from 1 year of MSG/SEVIRI rapid-scan images *Atmos. Chem. Phys.* **15** 8739–49
Voigt C *et al* 2021 Cleaner burning aviation fuels can reduce contrail cloudiness *Commun. Earth Environ.* **2** 114
Zhang D, Wang Z, Kollias P, Vogelmann A M, Yang K and Luo T 2018 Ice particle production in mid-level stratiform mixed-phase clouds observed with collocated A-Train measurements *Atmos. Chem. Phys.* **18** 4317–27